

Figure 3 Power difference between intrusion and no intrusion when pulse width is 125 ns. [Color figure can be viewed in the online issue, which is available at wileyonlinelibrary.com]

Figure 3(b), the power difference varies significantly when the distance D_1 is larger than 1000 m

In the traditional OTDR test, the numerical filtration of the signal from the noise is used to reduce the influence of the noise. The basic idea of this approach is that the noise is randomly distributed, and the average value of the noise component contained in the signal is zero. As a result, after many times' repetition of measurement process, the noise is automatically eliminated by averaging [8]. It can be shown that after the N times repeated measurements the signal to noise ratio (SNR) obtained by this signal processing is [8]:

$$\text{SNR} = \frac{\frac{1}{2} S \alpha_{rs} P_0 T_0 V_g e^{-2\alpha x} N}{P_{\text{NEP}} \sqrt{N}} \quad (6)$$

Here, P_{NEP} is the equivalent receiver noise, and N is the number of measurement repetitions. The other parameters are the same as Eq. (1). In this coherent system, besides the noise in Eq. (6), the SNR degradation caused by phase noise must be considered. In this case, Eq. (6) is rewritten as:

$$\text{SNR} = \frac{\frac{1}{2} S \alpha_{rs} P_0 T_0 V_g e^{-2\alpha x} N}{P_{\phi} + P_{\text{NEP}} \sqrt{N}} \quad (7)$$

P_{ϕ} is the equivalent phase noise. Because real time operation is required in intrusion detection system, the signal averaging measurement in traditional OTDR is inapplicable. From Eq. (7), we know SNR can be improved by a wider pulse. Although the greater the

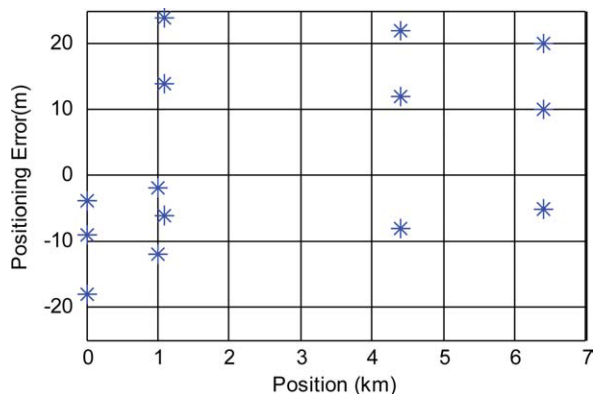


Figure 4 The positioning error in 1, 1008, 1084, 4392, and 6420 m with pulse width of 250 ns. [Color figure can be viewed in the online issue, which is available at wileyonlinelibrary.com]

pulse width the lower the positioning resolution is. When the optical pulse width is reduced to 125 ns, as demonstrated in Figure 3, the intrusion position $L = 1$ m is difficult to detect due to SNR reduction.

The positioning error is demonstrated in Figure 4, when the optical pulse width is 250 ns. The positions L of disturbance are 1 m, 1008, 1084, 4392, and 6420 m, respectively. The measured positioning errors are less than ± 25 m.

4. CONCLUSIONS

We have experimentally demonstrated an optical sensor system based on nonbalanced Mach-Zehnder interferometer and OTDR. The ± 25 m positioning resolution is demonstrated through experimental setup over an 8.8-km sensing fiber. A much longer sensing fiber is also applicable because OTDR can measure fiber of lengths up to ~ 200 km. Although the positioning resolution is difficult to improve due to SNR limitation when operating in a real time processing.

ACKNOWLEDGMENTS

This work was partly supported by Jiangsu Sensing Technologies Co. and 111 Project under Contract B07005.

REFERENCES

1. F. Xiaojun, A variable-loop Sagnac interferometer for distributed impact sensing, *J Lightwave Tech* 14 (1996), 2250–2254.
2. S.J. Russell, K.R.C. Brady, and J.P. Dakin, Real-time location of multiple time-varying strain disturbances, acting over a 40-km fiber section, using a novel dual-Sagnac interferometer, *J Lightwave Tech* 19 (2001), 205–213.
3. S.J. Spammer, P.L. Swart, and A.A. Chitchebakov, Merged Sagnac-Michelson interferometer for distributed disturbance detection, *J Lightwave Tech* 15 (1997), 972–976.
4. P.R. Hoffman and M.G. Kuzyk, Position determination of an acoustic burst along a Sagnac interferometer, *J Lightwave Tech* 22 (2004), 494–498.
5. J.C. Juarez, E.W. Maier, N.C. Kyoo, and H.F. Taylor, Distributed fiber-optic intrusion sensor system, *J Lightwave Tech* 23 (2005), 2081–2087.
6. E.E. Tapanes, Perimeter security system and perimeter monitoring method (PCT/AU02/0007), 2002.
7. K.I. Aoyama, K. Nakagawa, and T. Itoh, Optical time domain reflectometry in a single-mode fiber, *IEEE J Quant Electron* 17 (1981), 862–868.
8. F. Sischka, F. Newton, S.A. and M. Nazarathy, Complementary correlation optical time-domain reflectometry, *Hewlett Packard J* 12 (1988), 14–21.

© 2010 Wiley Periodicals, Inc.

DESIGN OF COMPACT MICROSTRIP ANTENNAS USING A MODIFIED GROUND PLANE

P. Mythili,¹ S. Mridula,¹ Binu Paul,¹ and P. Mohanan²

¹Division of Electronics, School of Engineering, Cochin University of Science and Technology, Kochi, Kerala, India; Corresponding author: mythili@cusat.ac.in

²Department of Electronics, Cochin University of Science and Technology, Kochi, Kerala, India

Received 9 March 2010

ABSTRACT: A method for simultaneously enhancing the bandwidth and reducing the size of microstrip antennas (MSAs) using a modified ground plane (GP) has been proposed with design formulas. A comb-shaped truncated GP is used for this purpose. This method provides an overall compactness up to 85% for proximity-coupled MSAs in the frequency range of 900 MHz–5.5 GHz with an improvement in

Key words: compact; microstrip antennas; modified ground plane; wide band; genetic algorithm

1. INTRODUCTION

There is an increase in demand for compact wideband antennas with improved performance for wireless communication applications. Microstrip antennas (MSAs) are widely used for this purpose because of their planar structure, low profile, light weight, moderate efficiency, and ease of integration with active devices. Almost all the important wireless applications lie in the band starting from 900 MHz to 5.5 GHz, which includes the GSM (880–960), GPS (1568–1592 MHz), DCS (1710–1880 MHz), and PCS (1850–1990 MHz), UMTS (1920–2170 MHz), IEEE 802.11 b/g (2400–2484), and WLAN IEEE 802.11a bands (5.15–5.35 GHz, 5.725–5.825 GHz). However, MSAs with normal ground plane (GP) offer narrow operating bandwidth [1]. Various techniques have been proposed by researchers to improve the compactness, bandwidth, gain, etc. of MSAs [2–10] by meandering or truncating the patch edges, adding parasitic patches, cutting slots on the radiating patch, using shorting pins, etc.

Very few works have been reported in the literature about the design of antennas to improve the compactness, bandwidth, radiation performance, etc. together without modifying the shape of the antenna.

In this article, a novel design technique that can be used to design compact and wideband antennas with a good radiation performance over various frequency bands within 900 MHz–5.8 GHz has been presented. Both regular- and arbitrary-shaped antennas can be designed with the help of a modified GP

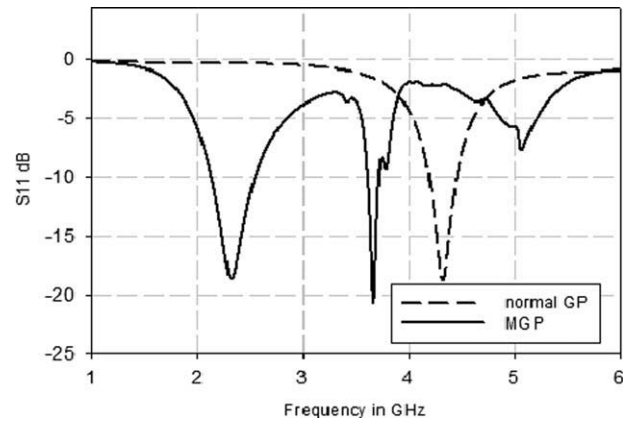


Figure 2 Return loss curves of the patch on the proposed GP with and without strips

(MGP), which has a rectangular ring with a double-sided comb structure. The ring structure with the strips helps in bringing down the resonant frequency and increase the bandwidth. Based on the study design, formulae have been obtained to find the dimensions of the MGP and a square patch for any frequency lying in the aforementioned band. These formulae can be extended for any regular-shaped patch. A detailed study has been done on the MGP for various strip lengths, widths, spacing, etc. Some of the antennas were fabricated and tested experimentally, which proves the validity of the design. HFSS and IE3D simulation softwares have been used for analysis.

2. ANTENNA CONFIGURATION

The proposed GP, the proximity-coupled antenna configuration, and the cross-sectional view along the feed are shown in Figure 1.

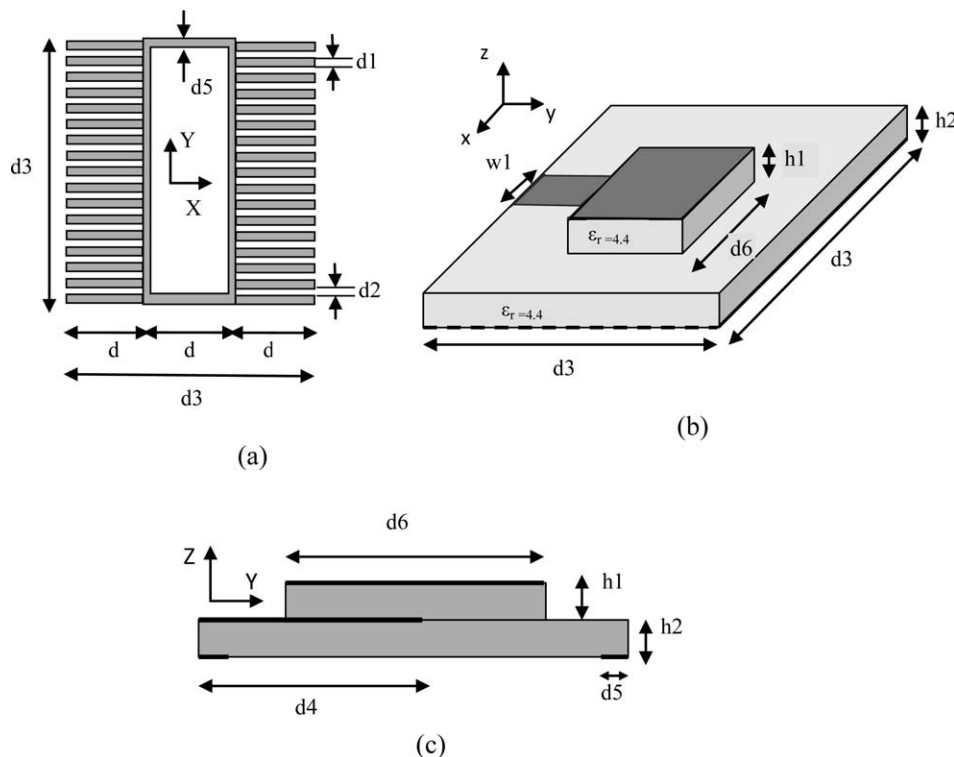


Figure 1 (a) Proposed double-sided comb structure on the ground plane. (b) Top view of the antenna with proximity coupling. (c) Cross-sectional view of the antenna

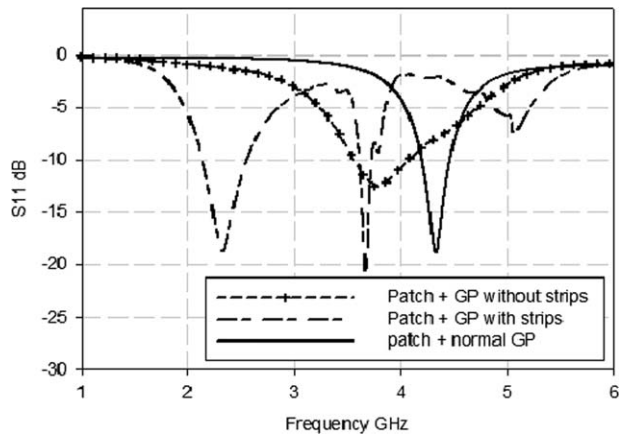
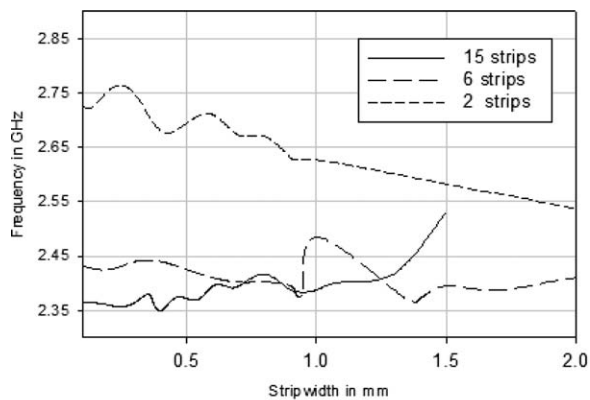
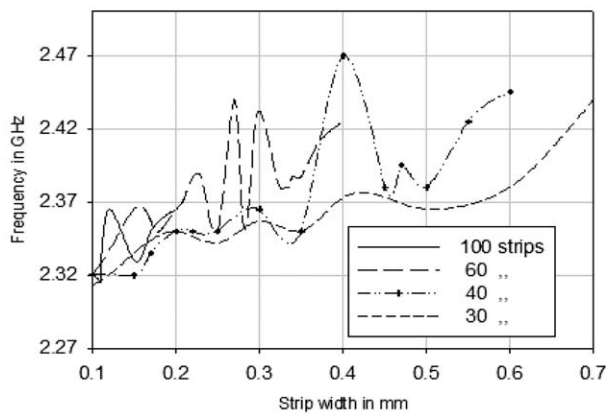


Figure 3 Return loss curves of $16 \times 16 \text{ mm}^2$ patch on normal GP and MGP of size $30 \times 30 \text{ mm}^2$

The MGP has a double-sided comb-like structure on the sides of a rectangular ring structure. The overall dimensions of the MGP are $d_3 \times d_3 \text{ mm}^2$. The inter strip spacing is $d_2 \text{ mm}$, and the width of the strip is $d_1 \text{ mm}$. The strip length and ring length are $d \text{ mm}$. The ring width is also $d_3 \text{ mm}$. The width of the feed is $w_1 = 3 \text{ mm}$, and its length d_4 is fixed as $d_3/2$, i.e., half the length of the MGP. The ring has a uniform width of $d_5 = 1 \text{ mm}$. The patch and the feed line are fabricated on a substrate of $\epsilon_r = 4.4$ and height $h_1 = h_2 = 1.6 \text{ mm}$. The dimension of the top patch is $d_6 \times d_6 \text{ mm}^2$.

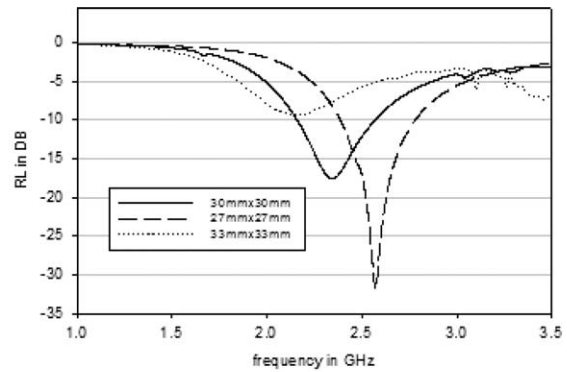


(a)

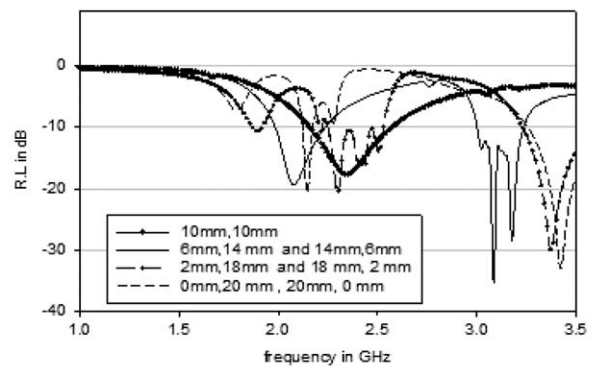


(b)

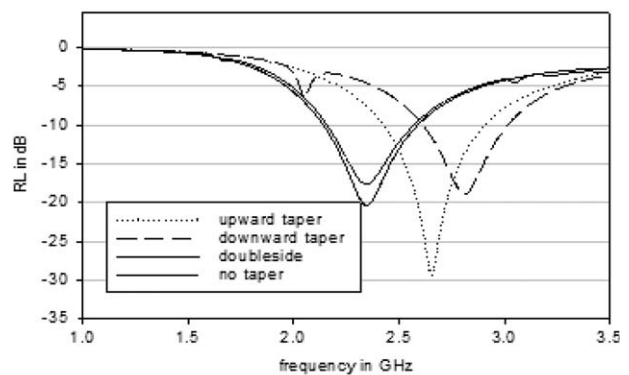
Figure 4 (a) Frequency vs. strip width for lesser number of strips. (b) Frequency vs. strip width for larger number of strips



(a)



(b)



(c)

Figure 5 (a) Effect of various GP sizes on resonance. (b) Effect of asymmetric strips on resonance. (c) Effect of taper on resonance

3. ANTENNA DESIGN AND ANALYSIS

The comb-shaped MGP acts like a frequency shifter and lowers the resonant frequency of the proximity-coupled MSA. The MGPs dimension can be calculated by the designer depending on the frequency of operation. Figure 2 shows the return loss (RL) of a patch antenna of size $16 \times 16 \text{ mm}^2$ on a normal GP and MGP of size ($d_3 \times d_3$) $30 \times 30 \text{ mm}^2$. It is evident from the figure that the antenna with MGP is resonating at 2.32 GHz compared with 4.4 GHz for a normal GP. It is interesting to note that the antenna with MGP is offering a bandwidth of 19%. An attempt has been made to understand the shift in frequency from 4.4 to 2.32 GHz with this proposed geometry that occupies the same volume. The proposed antenna is analyzed with the rectangular ring GP with and without strips. The RL curves of the aforementioned combinations are plotted in Figure 3. From the figure, it can be seen that the ring GP without strips brings

TABLE 1 Antenna Dimensions d_3 and d_6 (Actual and Using Equations), Bandwidth, and Compactness

Sl. No.	f (GHz)	d_6 (mm) (Actual)	d_6 (mm) Using Eq. (2)	d_3 (mm) (Actual)	d_3 (mm) Using Eq. (1)	% BW	% Compactness
1	0.90	44	44	66	66	19	56
2	1.45	29	28.7	45	44.2	20	59
3	1.80	23	22.7	36	36.7	25	64
4	2.31	16.4	16.9	30	29.5	19	69
5	3.7	8	8.3	18	18.2	15	80
6	4.4	5.7	6	15	15.1	10	82
7	4.9	4.8	4.7	13.5	13.4	8	85

down the resonance from 4.4 to 3.75 GHz. With the addition of strips, the resonance frequency further decreases. When the strip width is 0.15 mm, the frequency comes down to an extreme minimum of 2.32 GHz as shown in Figure 3 with the band from 2.1 to 2.57 GHz, i.e., 19% impedance bandwidth. The strips act as frequency shifters.

Variations of resonant frequency with various strip widths and spacing on the MGP are shown in Figures 4(a) and 4(b). It can be seen for a strip width of 0.15 mm (which is a reasonable size for fabrication) and 40 strips the resonant frequency of a rectangular patch can be brought down to a lowest of 2.32 GHz from 4.4 GHz. As the number of strips decreases, the frequency of resonance increases as shown in Figure 4(a). As the number of strips increases beyond 40, the variation of frequency with strip width is highly oscillatory. The traditional rectangular MSA for 2.4-GHz band requires a patch dimension of $29.5 \times 29.5 \text{ mm}^2$ on a normal GP of $50 \times 50 \text{ mm}^2$. The corresponding patch dimensions required for the same band were $16 \times 16 \text{ mm}^2$ on the proposed MGP of $30 \times 30 \text{ mm}^2$. This shows a reduction of 64% in the total area occupied by the patch compared with the conventional antenna. The BW increased to 19% when compared with 3% for the antenna on the normal GP.

The effect of varying MGP sizes, asymmetric strips, and tapered strips was also studied. The results are shown in Figure 5. From Figure 5(a), it can be seen that if MGP size increases the resonant frequency decreases. However, it is also noted that the antenna performance is considerably influenced by the MGP dimension. This means that there is an optimum MGP for better radiation performance. Figure 5(b) gives an idea on the performance of the antenna when the strips on both sides of the rectangular ring are asymmetric. Figure 5(c) indicates that the tapering of the comb also changes the resonant frequency of the system. It is found that an asymmetry of the comb increases the resonant

frequency. However, for a symmetric comb, the RL characteristic is almost identical to a nontapered comb structure. It can be observed that the resonance frequency lowers as the asymmetry increases but the bandwidth decreases. The maximum bandwidth occurs only when the strips are of same length. From the above observations, the strips were assumed to be of equal length without any asymmetry or taper. From exhaustive simulation and experimental studies, the following design equations were obtained.

$$d_3 = A + a_0 \cdot e^{-b_0 f} + c_0 \cdot e^{-d_0 f},$$

where $A = -0.3932$; $a_0 = 67.1313$; $b_0 = 1.6406$; $c_0 = 43.0567$; and $d_0 = 0.4370$ and

$$d_6 = B + a_1 \cdot e^{-b_1 f} + c_1 \cdot e^{-d_1 f},$$

where $B = 7.7866$; $a_1 = 152.4821$; $b_1 = 2.5975$; $c_1 = 68.8644$; and $d_1 = 0.5101$.

Table 1 shows the comparison between the antenna dimensions computed using the equation and the actual dimensions of the antenna. From the table, it can be seen that the % compactness increases with frequency and the % bandwidth initially increases, has a peak at 1.8 GHz and then decreases, but still the results are far better than the traditionally designed ones operating in the aforementioned ranges.

4. RESULTS AND DISCUSSION

The comparisons of simulated and experimental RL curves of the traditionally designed antenna and the compact antenna for 1.8 and 2.4 GHz are shown in Figures 6 and 7, respectively. A frequency of 1.8 GHz requires a patch dimension of $39 \times$

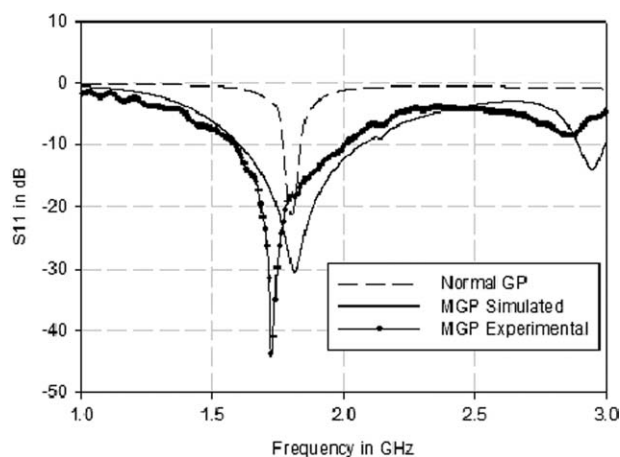


Figure 6 Comparison of RL curves for normal and proposed at 1.8 GHz

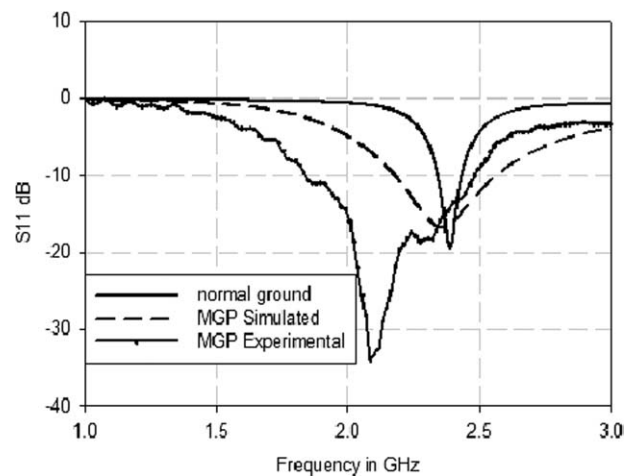


Figure 7 Comparison of RL curves for normal and proposed at 2.4 GHz

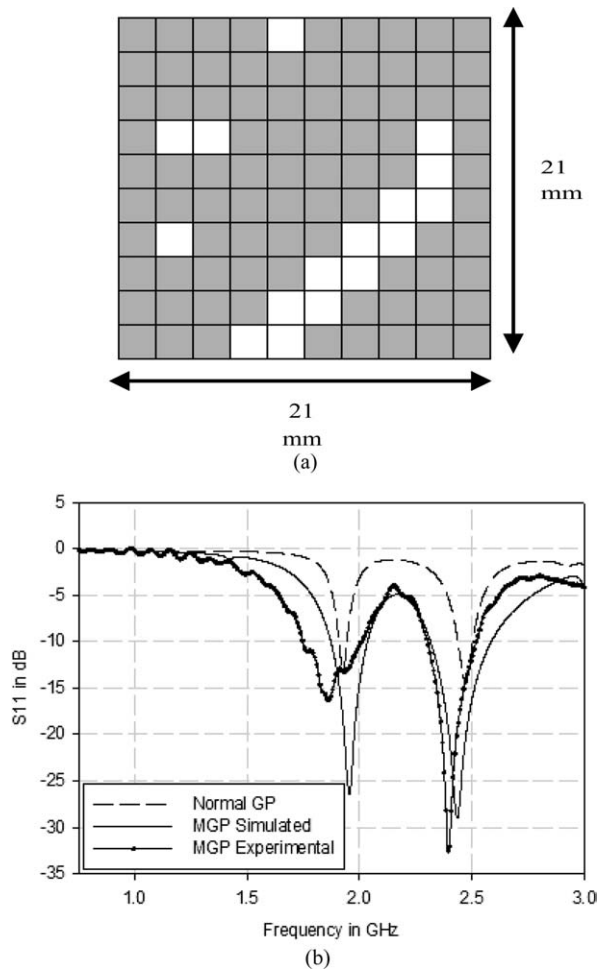


Figure 8 (a) Geometry of a wide dual-band genetic antenna. (b) Comparison of RL curves for a dual genetic antenna on normal and proposed GP

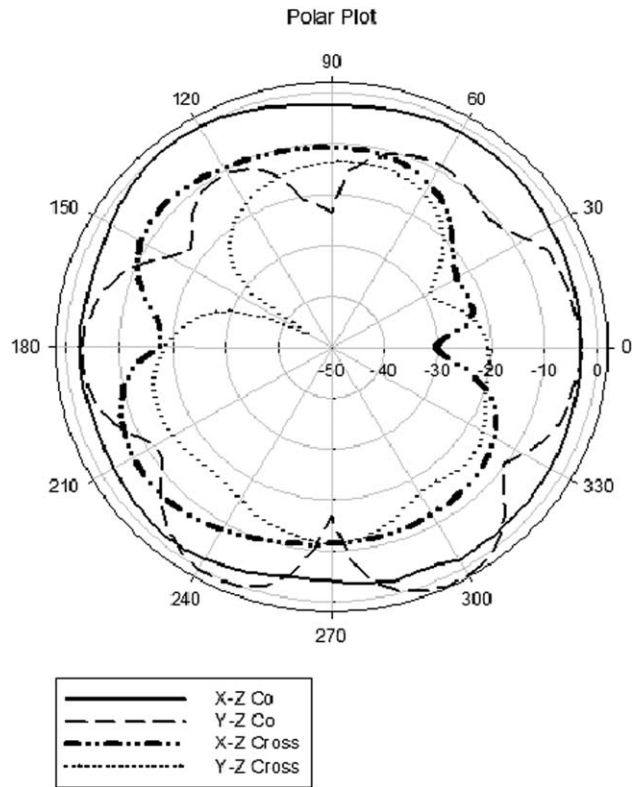


Figure 9 Radiation patterns for MSA designed for 2.4 GHz

39 mm² on a normal ground of size 60 × 60 mm² and has a BW of 4%. The same resonant frequency can be obtained by a patch size of 22 × 22 mm² on the proposed MGP of size 36 × 36 mm² (68% reduction in area) with a BW of 25% (simulation) and 30% (experiment). A similar improvement in bandwidth of about 19% (simulation) and 33% (experiment) with a reduction in area of 70% can be observed in Figure 7 for 2.4 GHz. The

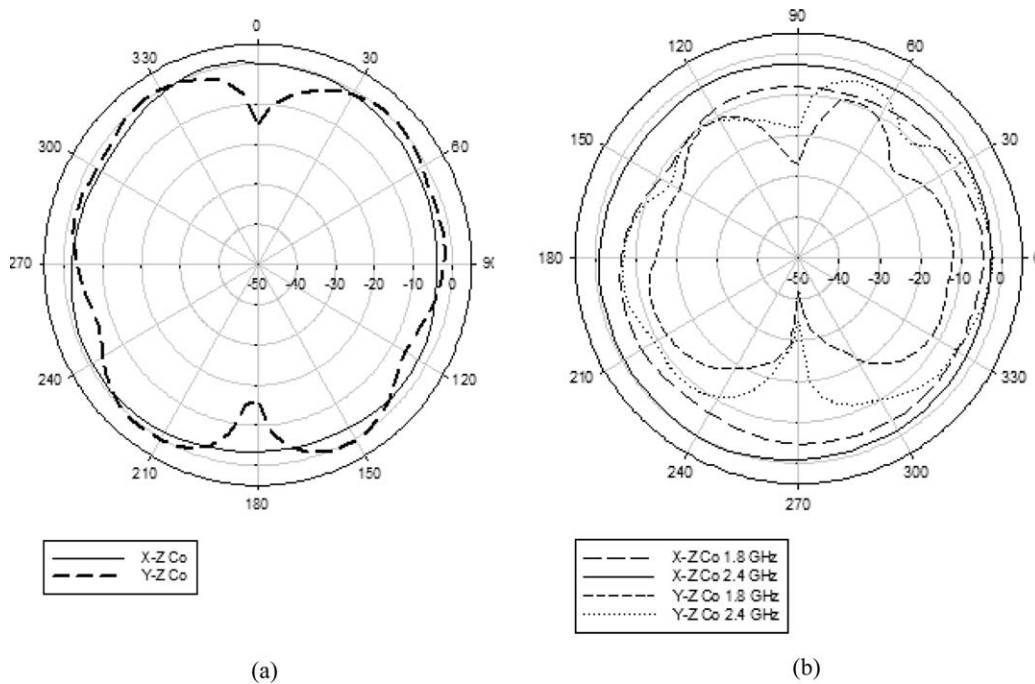


Figure 10 (a) Radiation patterns for the MSA designed for 1.8 GHz. (b) Radiation patterns for the genetic dual-band MSA at 1.8 and 2.4 GHz

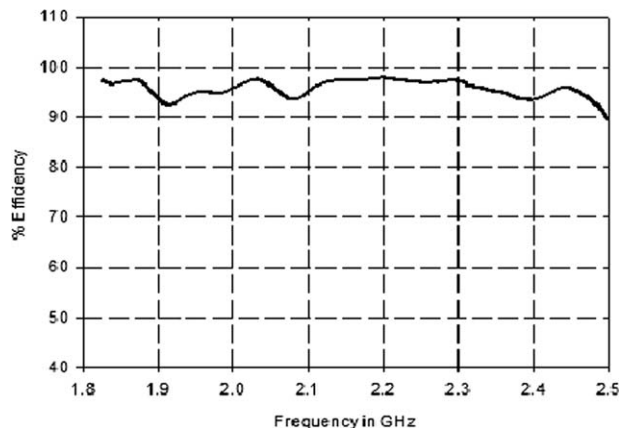


Figure 11 Measured antenna efficiency of the antenna designed for 2.4 GHz

performances of the antenna with other geometries are validated using experiment and simulation. One such example is highlighted in the next paragraph.

A dual-frequency antenna designed using GA with a normal GP ($50 \times 50 \text{ mm}^2$) had a patch size of $36 \times 36 \text{ mm}^2$. The antenna patch geometry is shown in Figure 8(a). The bandwidths of the antenna in the first two bands are 2 and 2.6%. However, it is worthwhile to note that the dimension of the antenna (with same geometry) required to provide the same resonance bands with MGP is only $21 \times 21 \text{ mm}^2$. In this case, the bandwidth was increased to 15 and 10% in the two bands. This has been demonstrated in Figure 8(b). Figure 9 shows the measured radiation pattern of the proposed antenna at 2.4 GHz. The XZ and YZ copatterns are almost omnidirectional. The radiation patterns of the antenna designed for 1.8 GHz and the dual-band genetic antenna are shown in Figures 10(a) and 10(b).

The difference between the measured and the theoretical RLs in the Figures 6–8 is due to the slight reduction in dimensions while fabricating the antennas. Even slight reductions or aberrations in the dimensions tend to reduce the resonant frequency as shown in Figure 4b. It can be seen from the figures that even though the resonant frequencies are reduced the bands are still maintained. The proposed antennas are compact and have a wider bandwidth compared with antennas reported in the literature [1–14]. The efficiencies of the antennas designed were measured using the Wheeler Cap method. The antenna efficiency of an antenna designed for 2.4-GHz operating frequency is shown in Figure 11.

5. CONCLUSION

A new method to design compact MSAs by modifying the GP has been proposed. This method is suitable for antennas with regular and arbitrary geometries. The presented design offers added advantage of increased bandwidth along with a compact structure.

ACKNOWLEDGMENTS

The authors thank the KSCSTE for the financial support and Miss Sandhya Rajan Project fellow for the timely help.

REFERENCES

1. K.L. Wong, Compact and broadband microstrip antennas, Wiley, New York, 2002.
2. S.S. Zhong and J.H. Cui, Compact dual frequency patch antennas, IEEE Trans Antennas Propag Soc Int Symp 4 (2001), 2196–2199.

3. Y.C. Lin and K.J. Hung, Compact ultra-wideband rectangular aperture antenna and band-notched designs, IEEE Trans Antennas Propag 54 (2006), 3075–3081.
4. K.L. Wong and S.C. Pan, Compact triangular microstrip antennas, Electron Lett 33 (1997), 433–434.
5. J. George, K.C. Anandan, P. Mohanan, and K.G. Nair, Analysis of a new compact microstrip antenna, IEEE Trans Antennas Propag 46 (1998), 1712–1717.
6. S.L. Latif, L. Shafai, and S.K. Shaema, Bandwidth enhancement and size reduction of microstrip slot antenna, IEEE Trans Antennas Propag 53 (2005), 994–1003.
7. W.S.T. Rowe and R.B. Waterhouse, Investigation of proximity coupled patch antennas suitable for MMIC integration, IEEE Antennas Propag Symp, Monterey, CA (2004), 1591–1594.
8. F. Yang, X.X. Zang, X. Ye, and Y. Rahmat Samii, Wide-band E shaped patch antenna for wireless communications, IEEE Trans Antennas Propag 49 (2001), 1094–1100.
9. J.Y. Sze and K.L. Wong, Slotted microstrip antenna for bandwidth enhancement, IEEE Trans Antennas Propag 48 (2005), 1149–1152.
10. S.Q. Xiao, B.Z. Wang, W. Shao, and Y. Zhang, Bandwidth enhancing ultra low profile compact patch antenna, IEEE Trans Antennas Propag 53 (2005), 3443–3447.
11. E.E.M. Khaled and A.R.R. Saad, Multi-wideband compact microstrip patch antenna based on slot matching, Prog Electromagn Res C 4 (2008), 169–177.
12. X.C. Yin, C.L. Ruan, S.G. Mo, C.Y. Ding, and J.H. Chu, A compact ultra-wideband and microstrip antenna with multiple notches, Prog Electromagn Res 84 (2008), 321–332.
13. C.-H. Lee, D.-H. Choi, and S.-O. Park, A novel compact and wide band shorted patch antenna, Microwave Opt Technol Lett 46 (2005), 4–6.
14. M. Joseph, B. Paul, R.K. Raj, and P. Mohanan, Compact wideband antenna for 2.4 GHz WLAN applications, Electron Lett 40 (2004), 1460–1461.

© 2010 Wiley Periodicals, Inc.

OPTICAL BISTABLE SWITCHING WITH SYMMETRICALLY CONFIGURED SOAs IN REVERSE BIAS

Pablo A. Costanzo-Caso,^{1,2} Michael Gehl,¹ Sergio Granieri,¹ and Azad Siahmakoun¹

¹Physics and Optical Engineering Department, Rose-Hulman Institute of Technology, 5500 Wabash Ave., Terre Haute, IN 47803; Corresponding author: siahmako@rose-hulman.edu

²Centro de Investigaciones Ópticas (CONICET La Plata- CIC) and Facultad de Ingeniería, Universidad Nacional de La Plata. Camino Centenario y 506, La Plata (1900), Argentina

Received 9 March 2010

ABSTRACT: A novel optical switching technique based on two symmetrically coupled semiconductor optical amplifiers operating in reverse-bias mode is proposed and experimentally demonstrated. The device produces both noninverted and inverted hysteresis behavior with switching speed in MHz range. However, switch performance can be improved by implementing this technique in a photonic integrated circuit. © 2010 Wiley Periodicals, Inc. Microwave Opt Technol Lett 52:2753–2759, 2010; View this article online at wileyonlinelibrary.com. DOI 10.1002/mop.25594

Key words: optical bistability; semiconductor optical amplifier (SOA); nonlinear effects

1. INTRODUCTION

Optical switching based on the fast nonlinear behavior of semiconductor optical amplifiers (SOA) has drawn a great deal of